

A Microstructurally-based Orthotropic Elasto-plastic Model for Paper and Paperboard

Phongphinitana E. and Jearanaisilawong P.*

Department of Mechanical and Aerospace Engineering, Faculty of Engineering, King Mongkut's University of Technology North Bangkok (KMUTNB), Bangkok, Thailand

Abstract

This report describes the formulation of a microstructurally-based orthotropic elastic-plastic continuum model for paper and paperboard. The model consists of two constitutive components: an elastic component developed from the finite deformation theory of elasticity, and a plastic component with a modified Tsai-Wu yield criteria and a nonlinear hardening function. Fiber orientation distribution underlying the paper structure is captured using a structural tensor. The model is implemented in a user-defined subroutine (UMAT) of a finite element software ABAQUS. Structural parameters of the model were measured from a selected set of papers using image analysis technique; other parameters were obtained from fitting the simulation results to the corresponding experimental data. Good agreements between the model predictions and the mechanical response of corrugated paperboard created from the selected set of papers confirm model validity.

Keywords: Paperboard, Finite Element Method, Fibrous Material, Fiber Orientation Distribution

1 Introduction

Paper and paperboard are the underlying load bearing structure for corrugated packages and containers. Thus, mechanical response of papers is the fundamental knowledge for package designers and manufacturers. With the emergence of finite element method, the process of designing and evaluating the strength of paper packages and containers can be efficiently performed using numerical simulations. To simulate the mechanics of paperboard structure requires part geometry, contact and boundary conditions, and most importantly an appropriate material model for papers.

Paper and paperboard exhibit dependence on loading direction and rate of deformation; the complex behaviour can be attributed to their underlying fiber network structure created during manufacturing process. Paper sheets are formed by collecting a slurry mixture of fibrils and starch on a moving belt. The mixture is then pressed and dried by a set of rollers creating a thin sheet where the alignment of fibers is biased along the direction of the press. Hence, the directional dependence of paper can be categorized into (1) the direction of machine or roll press (MD), (2) cross or perpendicular to the machine

direction (CD), and (3) out of plane direction (TD). Figure 1 shows the material directions in a paper roll.

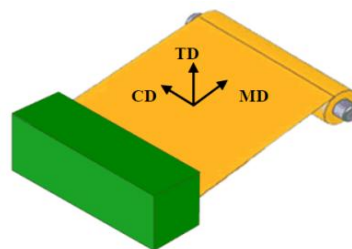


Figure 1: Directionality in a roll of paper [1]

Because the dimension of the paper thickness is smaller than the dimensions in the other directions, the mechanical response of paper sheets are analyzed under plane stress condition. In another word, the response is dominated by the in-plane stress components (MD-CD plane) while the out-of-plane stress components (TD direction) are insignificant. A representative plot of stress-strain curve of paper sheets under uniaxial tensile loading is demonstrated in Figure 2.

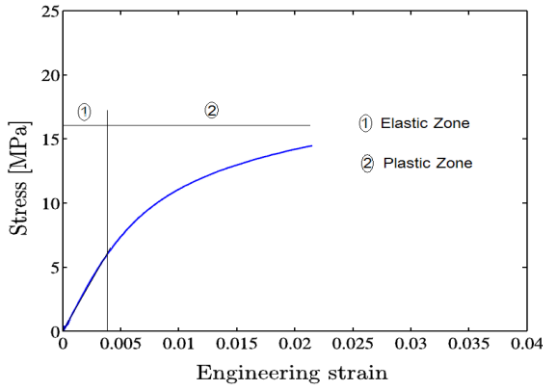


Figure 2: Representative response of paper under uniaxial tensile loading

The plot illustrates a behaviour characterized by a linear elastic zone representing a recoverable deformation due to stretching of fibers and starch matrix following by a nonlinear plastic zone corresponding to an unrecoverable deformation arising from a combination of fiber slip, fiber rupture and matrix breakage. Following the experimental observation, attempts to model paper sheets have focused on characterizing and modelling the complex nonlinear behaviour. Gilchrist et al. [2] modelled the nonlinear stress strain relation by the equation;

$$\sigma = C_1 \tanh(C_2 \varepsilon) + C_3 \varepsilon, \quad (1)$$

where σ is the stress component in one dimension,

ε is the strain component in one dimension,

C_1, C_2, C_3 are fitting constants.

Though Equation 1 is phenomenological in nature and only captures elastic response, this form of the stress-strain relation is accepted as an approximate response of paper sheets in one dimension. After the Gilchrist model, Makela et al. [3] proposed a constitutive model for paper sheets based on the classical linear elastic orthotropic model combined with Tsai-Wu failure criteria and a nonlinear hardening function in the form of Equation 1. Similar modelling approach has been employed by Mottola [1], Allansson and Sverd [4], Beldie [5], Haj Ali et al. [6] with various forms of hardening equations. Xia et al. [7] developed a new orthotropic yield surface and a hardening function specifically for paperboard. These models relied on phenomenological based orthotropic models that do not consider the effects of underlying fiber network structure.

Harrysson et al. [8] developed a micromechanics-based elastoplastic constitutive model for papers that includes the effect of network structure via a structural tensor. Harrysson model has been shown to capture the nonlinear responses of papers with various degrees of anisotropy. Yet the model requires a large set of model parameters for fitting the response, and the origin of structural tensor is still ambiguous. Thus, the objective of this work is to develop a constitutive model that incorporates the effects of fiber orientation via a structural tensor that is physically measurable from the underlying structure of paper sheets.

2 Experimental Investigation of In-plane response of Kraft Papers

2.1 Uniaxial tensile test

A selected grade of kraft paper provided by a local manufacturer is used as a representative material. To investigate the mechanical response of paper, a series of tensile tests was conducted on dogbone paper specimens along MD, CD, and 45 degree to the MD directions. A video extensometer was employed to measure paper elongation. The test was performed at a deformation rate of 2mm per minute until failure.

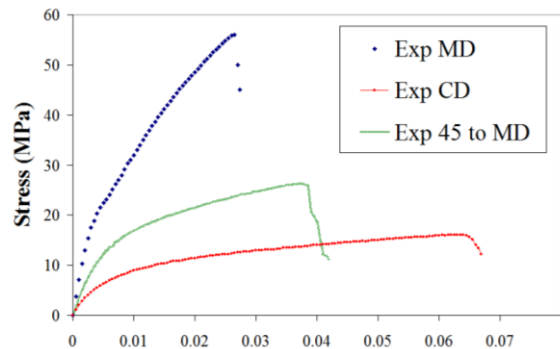


Figure 3: Stress-strain relation of the representative paper under uniaxial tension

The results in Figure 3 show that the test along the MD direction exhibits a stiffer response but a smaller elongation at break compared to that along the CD direction. The response along 45 degree to the MD direction falls between the CD and the MD with moderate stiffness and elongation at break. These results are consistent with the behaviour of paper sheets observed by other researchers.

2.2 Characterization of paper microstructure

An image of the representative paper sheets in Figure 4 was obtained using an optical microscope at 10 times magnification.

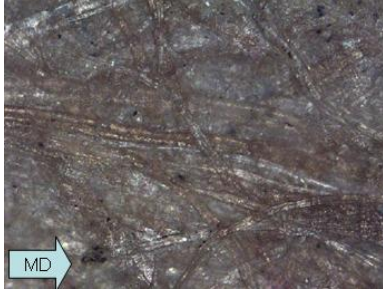


Figure 4: Microstructure of paper under an optical microscope

The image shows a network of fibers evenly distributed throughout the area of interest. The fibers are mostly straight with preferential alignment along the MD direction. The observations on paper microstructure coupled with the results of uniaxial tensile tests suggest that the material anisotropy in paper sheets is dominated by the orientation distribution of the constituent fibers. To quantify the fiber orientation distribution from the paper micrograph, an image analysis code following local orientation in image neighborhoods algorithm [9] was applied to the image in Figure 4 and additional 19 images taken from arbitrary locations of the same sheet. The averaged fiber orientation distribution of all images is shown in Figure 5.

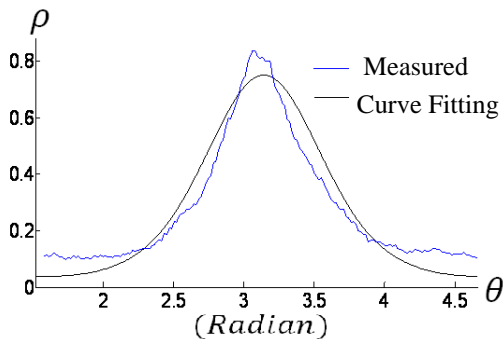


Figure 5: Fiber orientation distribution of the representative paper sheet

Following Gasser et al. [10], the fiber orientation distribution $p(\theta)$ is a probability density function

indicating the likelihood of fiber alignment in direction θ . Hence, $p(\theta)$ must be normalized to 1;

$$\frac{1}{2} \int_0^\pi \rho(\theta) \sin \theta d\theta = 1 \quad (2)$$

A structural tensor \underline{G} for a general two dimensional network structure is constructed from

$$\underline{G} = \begin{bmatrix} g_{11} & g_{12} \\ g_{12} & g_{22} \end{bmatrix} = h \underline{I} + (1-2h) \underline{a}_0 \otimes \underline{a}_0 \quad (3)$$

where g_{11}, g_{12}, g_{22} are the components of the structural tensor, \underline{a}_0 is the unit vector indicating the preferential direction of fibers, \underline{I} is a 2 by 2 identity matrix, and $h = \frac{1}{2} \int_0^\pi \rho(\theta) \sin^3 \theta d\theta$. The fiber orientation

is assumed to be distributed according to a π -periodic von Mises distribution given by;

$$\rho(\theta) = 4 \sqrt{\frac{b}{2\pi}} \frac{\exp[b \cos(2\theta) + 1]}{\text{erfi}(\sqrt{2b})} \quad (4)$$

where b denotes the concentration parameter of the fiber orientation and $\text{erfi}(x) = -i \text{erf}(ix)$ is an imaginary error function. Thus, the structural tensor can be determined by fitting the parameter b to the experimentally measured fiber orientation distribution. The value of b in Figure 5 is 1.5.

3 Continuum mechanics framework

3.1 Kinematics

A continuum body B_0 in the reference configuration is filled with infinitesimal volume elements whose position of each element is denoted by a vector \underline{X} . The motion of the element is described by a one-to-one, generally nonlinear, mapping function $\underline{x} = \underline{x}(\underline{X}, t)$, where \underline{x} denotes the position of element \underline{X} at time t of the body B_t in the current configuration. The deformation of such body can be determined from a linear map known as a deformation gradient \underline{F} ;

$$\underline{F} = \frac{d\underline{x}}{d\underline{X}} \quad (5)$$

which describes the transformation of a material line $d\underline{X}$ in the reference configuration into its counterpart $d\underline{x}$ in the deformed configuration. For a

unique deformation, the Jacobian of the linear map must be positive;

$$J = \det(\underline{F}) > 0. \quad (6)$$

Time derivative of the deformation gradient is related to a spatial velocity gradient \underline{L} via

$$\dot{\underline{F}} = \underline{L}\underline{F}. \quad (7)$$

The spatial velocity gradient may be split into a symmetric part \underline{D} and a skew-symmetric part \underline{W} according to

$$\underline{L} = \underline{D} + \underline{W}, \quad (8)$$

where $\underline{D} = \frac{1}{2}(\underline{L} + \underline{L}^T)$ is a stretch rate tensor and

$$\underline{W} = \frac{1}{2}(\underline{L} - \underline{L}^T) \text{ is a spin tensor.}$$

Following Kroner-Lee decomposition, the deformation gradient of an elastoplastic body may be decomposed into an elastic deformation gradient \underline{F}^e and a plastic deformation gradient \underline{F}^p according to

$$\underline{F} = \underline{F}^e \underline{F}^p. \quad (9)$$

The mapping of the Jacobian is also decomposed into an elastic part and a plastic part according to

$$J = J^e J^p; \quad J^e = \det(\underline{F}^e); \quad J^p = \det(\underline{F}^p) \quad (10)$$

The decomposition map in Equation 10 is shown in Figure 6.

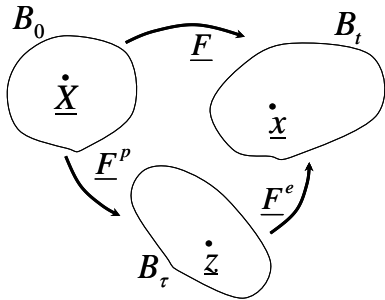


Figure 6: Deformation map of a continuum body

where \underline{z} denotes the position of element \underline{X} in the relaxed configuration B_τ . The relaxed configuration is non-physical but serve as an idealization of relaxed state of the body after being unloaded from the elastic deformation. The elastic velocity gradient and the plastic velocity gradient are defined by

$$\dot{\underline{F}}^e = \underline{L}^e \underline{F}^e; \quad \dot{\underline{F}}^p = \underline{L}^p \underline{F}^p. \quad (11)$$

The spatial velocity gradient can be decomposed into an elastic velocity gradient \underline{L}^e , and a plastic velocity gradient \underline{L}^p ;

$$\underline{L} = \underline{L}^e + \underline{F}^e \underline{L}^p \underline{F}^{e-1}. \quad (12)$$

The elastic velocity gradient is defined in the current configuration, while the plastic velocity gradient is defined in the relaxed configuration.

3.2 Thermodynamics

Constitutive models describing the material behaviour must comply with the laws of Thermodynamics. Specifically, the 1st and 2nd laws of thermodynamics are written in a combined form as the reduced dissipation inequality, which for isothermal conditions is given by,

$$\frac{1}{2} \underline{S} : \dot{\underline{C}} - \dot{\psi} \geq 0, \quad (13)$$

where \underline{S} is the second Piola-Kirchhoff stress tensor, $\underline{C} = \underline{F}^T \underline{F}$ is the right Cauchy Green tensor, ψ is the Helmholtz free energy. For the proposed model, the change in Helmholtz free energy of the system is due to the contribution of the elastic deformation of the body

$$\psi = \psi(\underline{C}^e), \quad (14)$$

where $\underline{C}^e = \underline{F}^{eT} \underline{F}^e$ is the elastic right Cauchy green tensor. Substituting Equation (14) into (13) yields

$$\left(\frac{1}{2} \underline{S} - \underline{F}^{p-1} \frac{\partial \psi(\underline{C}^e)}{\partial \underline{C}^e} \underline{F}^{p-T} \right) : \dot{\underline{C}} + 2 \frac{\partial \psi(\underline{C}^e)}{\partial \underline{C}^e} \underline{C}^e : \underline{L}^p \geq 0 \quad (15)$$

From separation hypothesis, Equation 15 may be split into elastic contribution;

$$\underline{S} = 2J^p \underline{F}^{p-1} \frac{\partial \psi(\underline{C}^e)}{\partial \underline{C}^e} \underline{F}^{p-T}, \quad (16)$$

and dissipative contribution;

$$\underline{\Xi} : \underline{L}^p \geq 0. \quad (17)$$

where $\underline{\Xi} = \frac{\partial \psi(\underline{C}^e)}{\partial \underline{C}^e} \underline{C}^e$ is the Mendel stress tensor.

An elasto-plastic model is completed by specifying the Helmholtz free energy and an evolution law for plastic velocity gradient. One possibility of the evolution laws (among many others) is to define a convex potential function $f(\underline{\Xi})$ such that

$$\underline{L}^p = \lambda \frac{\partial f}{\partial \underline{\Xi}} \quad (18)$$

where λ is a positive multiplier. The evolution law in Equation 18 is referred to as associative plasticity theory, in conjunction with the maximum plastic dissipation postulate. The Cauchy stress tensor is

then given by a push-forward operation of Equation 16.

$$\underline{\sigma} = \frac{1}{J} \underline{F} \underline{S} \underline{F}^T = \frac{2}{J^e} \underline{F}^e \frac{\partial \psi(\underline{C}^e)}{\partial \underline{C}^e} \underline{F}^{eT} \quad (19)$$

3.3 Application to paper and paperboard

Paper and paperboard are thin sheet structures, and their mechanical responses can be modelled by plane stress. Further, their out-of-plane response is considered decoupled from the in-plane response, and the out-of-plane deformation is described by a simple linear elastic model. Hence, this work focuses on the modelling of the in-plane mechanics of paper and paperboard.

We assume that the directionality of the in-plane response of this material is solely governed by the effect of biased fiber orientation, and that the material is sufficiently thin that the in-plane fiber orientation distribution of the structure is represented by the fiber orientation distribution on its surface. Therefore, the structural tensor representing fiber orientation distribution described in Section 2.2 can be used for capturing the directionality of the mechanical response of paper and paperboard. Further, the underlying structure of the material is not damaged; and therefore, the structural tensor remains unchanged with the deformation.

Following the continuum mechanics framework, the free energy is formulated based on the theory of invariant with the structural tensor served as material parameters. In this model, the following form of Helmholtz free energy is proposed:

$$\psi = k_1(J_1 - 1) + k_2(J_1 - 1)^2 + k_3(J_2 - 1) + \kappa J_3 \ln J_3 \quad (20)$$

where J_1 , J_2 , and J_3 are invariants of \underline{C}^e and \underline{G} defined by

$$\begin{aligned} J_1 &= \text{trace}(\underline{C}^e \underline{G}) \\ J_2 &= \text{trace}(\underline{C}^{e-1} \underline{G}) \\ J_3 &= \det(\underline{C}^e) \end{aligned} \quad (21)$$

and k_1 , k_2 , k_3 and κ are material parameters.

Using Equation 19, 20 and 21, the Cauchy stress of the proposed model is given by

$$\underline{\sigma} = \frac{2}{J^e} \left[k_1 \left(\underline{F}^e \underline{G} \underline{F}^{eT} - \underline{F}^{e-T} \underline{G} \underline{F}^{e-1} \right) + \left[k_2(J_1 - 1) \underline{F}^e \underline{G} \underline{F}^{eT} + J^e \kappa \ln(J^e) \underline{1} \right] \right] \quad (22)$$

Note that for equilibrium consideration, $\underline{\sigma}(\underline{C}^e = \underline{1}) = \underline{0}$ and therefore, $k_1 = k_3$.

To model plasticity, an evolution law of the plastic velocity gradient must be defined via a potential function. Tsai-Wu model [11] used an anisotropic yield function that is a generalization of Hill criteria for isotropic material. In this work, a modification of Tsai-Wu yield criteria will be adopted for the in-plane plasticity of paperboard. The potential function is given by

$$f = \frac{1}{S} \left(a_{11} g_{11}^2 \Xi_{11}^2 + a_{22} g_{22}^2 \Xi_{22}^2 + 2a_{12} g_{11} g_{22} \Xi_{11} \Xi_{22} \right) + b(g_{11} + g_{22}) \Xi_{12}^2 \quad (23)$$

where Ξ_{ij} are the in-plane components of the Mendel stress tensor, g_{ij} are the in-plane components of the structural tensor, S is a strength-like parameter, a_{11} , a_{22} , a_{12} and d are model parameters. The yield function represents the onset of plastic deformation. To capture the non-linear response post-yielding, a hardening function is introduced to the parameter S . We assume that the resistance of the structure to plastic yielding S evolves with the level of effective plastic strain rate defined by

$$\dot{\epsilon}_{eff}^p = \sqrt{\underline{D}^p : \underline{D}^p} \quad (24)$$

The hardening function is chosen as

$$S = S_0 + c_1 \tanh(c_2 \dot{\epsilon}_{eff}^p) + c_3 \dot{\epsilon}_{eff}^p \quad (25)$$

where S_0 is the initial strength, c_1, c_2, c_3 are fitting parameters. The model requires 14 parameters $k_1, k_2, \kappa, g_{11}, g_{12}, g_{22}, a_{11}, a_{22}, a_{12}, c_1, c_2, c_3, b, S_0$ to completely describe the elastoplastic response of paper and paperboard under in-plane loads.

4 Results and Discussions

The proposed model was implemented in a commercially available finite element software ABAQUS via user material subroutine (UMAT). To validate the model, a set of finite element simulations with the same geometry and loading conditions as the uniaxial tensile tests were generated using 1st order reduced integration shell (S4R) elements.

The material parameters of the model were obtained using the following procedure. The components of the structural tensor g_{11}, g_{12}, g_{22} were measured from the paper structure using the image analysis technique described in Section 2.2. The parameters corresponding to the elastic components of the model k_1, k_2, κ were fitted to the linear zone of the tensile test result in the CD direction, while the initial

strength S_0 and model parameters a_{11}, a_{22}, a_{12} and b are obtained by calibrating the onset of plastic deformation of both the MD and the CD directions. Lastly, the plastic hardening parameters are fitted to the nonlinear portion of the test result in the CD direction only. Table 2 shows the model parameters used in the simulation.

Table 2: Model parameters for the representative paper

$k_1 = 1.0 \text{ GPa}$	$k_2 = 5.6 \text{ GPa}$	$\kappa = 1.0 \text{ kPa}$
$g_{11} = 0.729$	$g_{12} = 0$	$g_{22} = 0.271$
$a_{11} = 0.03$	$a_{12} = -0.1$	$a_{22} = 1$
$b = 0.037$	$S_0 = 13.36 \text{ MPa}$	$c_1 = 7.14 \text{ MPa}$
$c_2 = 150 \text{ sec}^{-1}$	$c_3 = 216.67 \text{ MPa}(\text{sec})^{-1}$	

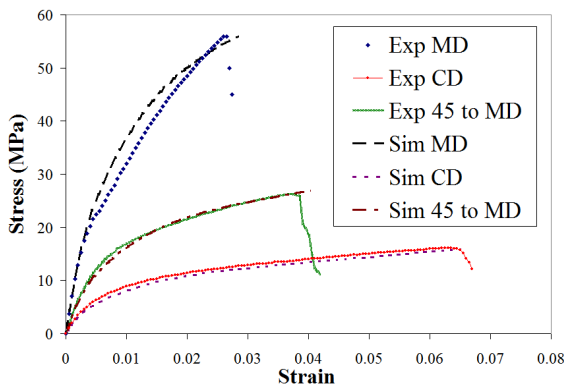


Figure 7: Model predictions compared to experimental results

Stress-strain curves along the MD, CD and 45 degree to MD directions predicted by the simulations are compared to the corresponding experimental results in Figure 7. The model is shown to capture the linear elastic response, the onset of plastic deformation, and the plastic hardening behaviour of all three material directions. Slight discrepancies are observed in the prediction along the MD direction as the MD response is predicted from fitted parameters in the CD direction. In summary, good agreements between the experimental results and the predictions by the simulations confirm the validity of the proposed constitutive model formulation.

5 Conclusions

An elastoplastic constitutive model for the in-plane response of paper sheets has been proposed. The proposed model requires 14 parameters to capture the nonlinear and directional dependent response of this material. The underlying network structure of paper is captured in the model via a physically measurable structural tensor. The model is shown to capture the complex nonlinear elastoplastic behaviour of paper and paperboard under in-plane loading conditions.

Acknowledgments

This project is supported by New Researcher scholarship by Coordinating Center for Thai Government Science and Technology Scholarship Students (CSTS), National Science and Technology Development Agency (NSTDA), Thailand.

References

- [1] Mottola, E., 2001. *Design models for corrugated board packaging*, Master Dissertation, Lund University.
- [2] Gilchrist, A.C., Suhling, J.C., and Urbanik, T.J., 1999. *Nonlinear finite element modeling of corrugated board*, Mechanics of Cellulosic Materials, AMD-Vol. 231/MD-Vol. 85, ASME.
- [3] Makela, P., Ostlund, S., 2003. *Orthotropic elastic-plastic material model for paper materials*, International Journal of Solids and Structures, 40: 5599-5620.
- [4] Allansson, A., and Svard, B., 2001. *Stability and collapse of corrugated board; numerical and experimental analysis*, Master Dissertation, Lund University.
- [5] Beldi, L., 2001. *Mechanics of paperboard packages – Performance at short term static loading*, Licentiate Dissertation, Lund University.
- [6] Haj-Ali, R., Choi, J., Wei, B.S., Popil, R., Schaepe, M., 2009. *Refined nonlinear finite element models for corrugated fiberboards*, Composite Structures 87:321-333.
- [7] Xia, Q.S., Boyce, M.C., Parks, D.M., 2002. *A constitutive model for the anisotropic elastic-plastic deformation of paper and paperboard*, International Journal of Solids and Structures 39: 4053-4071.

- [8] Harrysson, A., Ristinmaa, M., 2008. *Large strain elasto-plastic model of paper and corrugated board*, International Journal of Solids and Structures, 45: 3334–3352.
- [9] Jaehne B., 2005. *Digital Image Processing*, 6th Edition, Springer.
- [10] Gasser, T.C., Ogden, R.W., and Holzapfel, G.A. 2006. *Hyperelastic Modelling of Arterial Layers with Distributed Collagen Fibre Orientations*, Journal of Royal Society Interface, 3:13 – 35.
- [11] Tryding, J., 1994. *A modification of the Tsai-Wu failure criterion for the biaxial strength of paper*, Tappi Journal 77(8): 132-134.